efficient of variation for the frequency of the specific point mutations of ~20%, supporting the reproducibility of the estimates. Therefore, it is possible that the observed decrease in the T414G mutation frequency in the LS6-82 y sample results from a difference in the biopsy site or from handling of the original specimen.
29. The method for allele-specific termination of primer extension is described in (*38*).
30. Y. Michikawa and G. Attardi, data not shown.
31. N. B. Reuven, G. Tomer, Z. Livneh, *Mol. Cell* **2**, 191 (1998).
32. M. Yoneda, A. Chomyn, A. Martinuzzi, O. Hurko, G. Attardi, *Proc. Natl. Acad. Sci. U.S.A.* **89**, 11164 (1992).
33. N.-G. Larsson, E. Holme, B. Kristiansson, A. Oldfors, M. Tulinius, *Pediatr. Res.* **28**, 131 (1990).
34. K. Polyak *et al.*, *Nature Genet.* **20**, 291 (1998).
35. S. C. Ghivizzani, C. S. Madsen, M. R. Nelen, C. V. Ammini, W. W. Hauswirth, *Mol. Cell. Biol.* **14**, 7717 (1994).
36. R. P. Fisher, T. Lisowsky, M. A. Parisi, D. A. Clayton, *J. Biol. Chem.* **267**, 3358 (1992).
37. D. Y. Lee and D. A. Clayton, *Genes Dev.* **11**, 582 (1997); *J. Biol. Chem.* **273**, 30614 (1998).
38. Supplemental material is available at the *Science* Web site (www.sciencemag.org/feature/data/1040395.shl).
39. Supported by National Institute on Aging (NIH) grant AG12117-03 (to G.A.). We thank A. Chomyn and G. Villani for valuable discussions, M. Lai for support, A. Aman, R. Steinberger, and M. Scott for their help with experiments, and A. Drew, B. Keeley, R. Zedan, and C. Lin for expert technical assistance.

26 March 1999; accepted 14 September 1999

Crystal Structure of the Ectodomain of Human Transferrin Receptor

C. Martin Lawrence,[1,2] Sanjoy Ray,[1]* Marina Babyonyshev,[1] Renate Galluser,[1] David W. Borhani,[1]† Stephen C. Harrison[1,2]‡

The transferrin receptor (TfR) undergoes multiple rounds of clathrin-mediated endocytosis and reemergence at the cell surface, importing iron-loaded transferrin (Tf) and recycling apotransferrin after discharge of iron in the endosome. The crystal structure of the dimeric ectodomain of the human TfR, determined here to 3.2 angstroms resolution, reveals a three-domain subunit. One domain closely resembles carboxy- and aminopeptidases, and features of membrane glutamate carboxypeptidase can be deduced from the TfR structure. A model is proposed for Tf binding to the receptor.

The transferrin receptor (TfR) assists iron uptake into vertebrate cells through a cycle of endo- and exocytosis of the iron transport protein transferrin (Tf) (*1*). TfR binds iron-loaded (diferric) Tf at the cell surface and carries it to the endosome. Iron dissociates from Tf upon acidification of the endosome, but apo-Tf remains tightly bound to TfR. The complex then returns to the cell surface. At extracellular pH, apo-Tf dissociates and is replaced by diferric Tf from serum. This cycle has become one of the most widely studied models for receptor-mediated endocytosis.

Human TfR is a homodimeric type II transmembrane protein. The 90-kD subunit has a short, NH_2-terminal cytoplasmic region (residues 1 to 67), which contains the internalization motif YTRF (*2*), a single transmembrane pass (residues 68 to 88), and a large extracellular portion (ectodomain, residues 89 to 760), which contains a binding site for the 80-kD Tf molecule. Electron cryomicroscopy shows that the TfR dimer has a globular, extracellular structure separated from the membrane by a stalk of about 30Å (*3*). The stalk presumably includes residues immediately following the transmembrane pass and the O-linked glycan at Thr^{104} [see (*4*) and references therein] as well as two intermolecular disulfide bonds—one formed by Cys^{89} and one formed by Cys^{98} (*5*). The intermolecular disulfides are not required for dimerization (*6*). Treatment of TfR-containing membranes with trypsin releases a soluble fragment, residues 121 to 760, whose crystallization has been described (*7*). The released receptor is a dimer. It binds two molecules of Tf with normal affinity and it corresponds to the large globular structure shown by electron microscopy. A similar fragment is found as a normal component of human serum; its level is inversely correlated with body iron stores (*4*). HFE, the product of the gene responsible for human hereditary hemochromatosis (tissue iron overload) and a homolog of the heavy chain of class I major histocompatibility complex molecules, has recently been identified as a second ligand for TfR (*8*). Hereditary hemochromatosis is the most common genetic disease among persons of northern European descent. Association with HFE lowers the affinity of TfR for Tf by a factor of 10 to 50 (*8*) and also appears to impede dissociation of iron from Tf in the endosome (*9*).

The amino acid sequence of the globular ectodomain of TfR is 28% identical to that of membrane glutamate carboxypeptidase II (mGCP). mGCP hydrolyzes *N*-acetyl-α-L-aspartyl-L-glutamate, the most prevalent mammalian neuropeptide (*10*). Several groups have noticed the similarity of mGCP to aminopeptidases, and one group has extended this analysis to TfR, suggesting that TfR evolved from a peptidase related to mGCP (*11*). In TfR, three of the presumed Zn ligands of the predicted protease-like domain are missing, and TfR lacks peptidase activity.

We have expressed an equivalent of the tryptic fragment of human TfR in Chinese hamster ovary (CHO) cells (*12*) and determined its structure at 3.2 Å resolution (*13*). Because crystals of TfR diffract significantly better after soaking in $SmCl_3$, we determined the structure of TfR in the presence of bound Sm^{3+} ions. The asymmetric unit of the crystals contains four TfR dimers (8 × 70 kD = 560 kD) stacked in an 8_5 helical array coincident with a crystallographic 2_1 axis (*14*). We have found interpretable electron density for the entire tryptic fragment except for Arg^{121} at the NH_2-terminus. We also see density for the first *N*-acetylglucosamine residue at each of the three N-linked glycosylation sites (*15*).

The TfR monomer contains three distinct domains, organized so that the TfR dimer has a butterfly-like shape (Fig. 1). The positions of the NH_2-termini allow orientation of TfR with respect to the plasma membrane. Secondary structural elements for each domain are shown in Fig. 2; the notation used below is explained in the legend. The first, protease-like domain contains residues 122 through 188 and 384 through 606. Its fold, which is closely related to that of carboxy- or aminopeptidase (*16*), has a central, seven-stranded, mixed β sheet with flanking α helices (Fig. 2A). Carboxypeptidase itself has eight β strands, but in TfR the polypeptide chain traces a path away from the outside edge of the β sheet, forming an extended loop (α1–7/α1–8). A disulfide bond within the protease-like domain is unusual in linking Cys^{556} and Cys^{558}, only two residues apart at the end of βI-6.

The second, apical domain contains residues 189 to 383. It resembles a β sandwich in which the two sheets are splayed apart (Fig. 2B), with a helix (αII-2) running along the open edge. A related structure has been seen in domain 4 of aconitase (*17*). An extended segment of polypeptide connects βII-6 and βII-7, traversing the interface between the apical and protease-like domains. At the COOH-terminus of this apical traverse is a

[1]Howard Hughes Medical Institute and Children's Hospital Laboratory of Molecular Medicine, 320 Longwood Avenue, Boston, MA 02115, USA. [2]Department of Biological Chemistry and Molecular Pharmacology, Harvard Medical School, Boston, MA 02115, USA.

*Present address: Whitehead Institute, 9 Cambridge Center, Cambridge, MA 02142, USA.
†Present address: Department of Organic Chemistry, 2000 Ninth Avenue South, Southern Research Institute, Birmingham, AL 35205, USA.
‡To whom correspondence should be addressed. E-mail: harrison@crystal.harvard.edu

large loop with residues (Asp^{307} and Thr^{310}) that help sequester one of the Sm^{3+} ions, in conjunction with Glu^{465} and Glu^{468} from αI-5 of the protease-like domain. The Sm^{3+}-liganding loop also interacts with αIII-6 across the dimer interface.

With respect to the linear sequence, the apical domain is an insert between the first and second strands of the central β sheet in the protease-like domain. Packing interactions within the crystal, which in several places involve βII-2 and the reverse turn between βII-1 and βII-2, result in slightly different orientations of the apical domain in each of the eight monomers in the asymmetric unit. The β strands running between the protease-like domain and the apical domain act as a hinge, allowing small rotations (2°) of one domain with respect to the other (arrows, Fig. 1). Greater rotations of the apical domain may be possible in solution, in the absence of Sm^{3+}, or at a different pH.

The third, helical domain (Fig. 2C) contains residues 607 through 760. It is best described as a four-helix bundle formed by a pair of parallel α-hairpins, with the first and third helices of the bundle each broken in two. Thus, αIII-1 and αIII-2 correspond to the first helix of the bundle, and αIII-4 and αIII-5 correspond to the third. The large loop-like insert between αIII-4 and αIII-5 has an important structural role. Within a monomer, this loop contacts the Sm^{3+}-binding loop of the apical domain and helix αI-8 of the protease-like domain. It also interacts with its counterpart across the molecular twofold axis. Indeed, one principal function of the helical domain appears to be TfR dimerization; it contacts each of the three domains in the dimer partner. These interactions include contacts with the Sm^{3+}-binding loop in the partner's apical domain. A second Sm^{3+} site lies between the body of domain III and the poorly ordered COOH-terminal tail of the polypeptide chain.

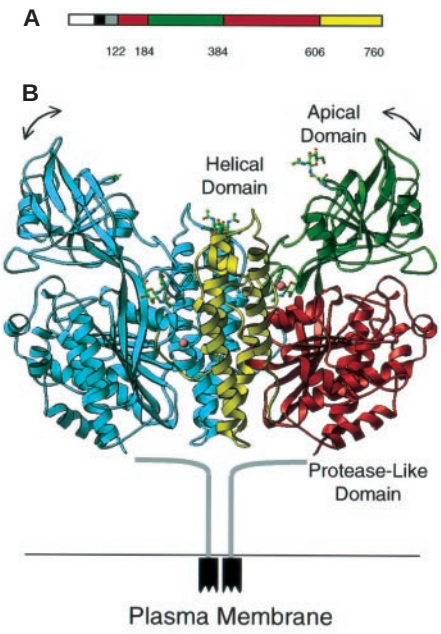

Fig. 1. Structure of the ectodomain of the TfR. (**A**) Domain organization of the TfR polypeptide chain. The cytoplasmic domain is white; the transmembrane segment is black; the stalk is gray; and the protease-like, apical, and helical domains are red, green, and yellow, respectively. Numbers indicate residues at domain boundaries. (**B**) Ribbon diagram of the TfR dimer depicted in its likely orientation with respect to the plasma membrane. One monomer is colored according to domain (standard coloring as described above), and the other is blue. The stalk region is shown in gray connected to the putative membrane-spanning helices. Pink spheres indicate the location of Sm^{3+} ions in the crystal structure. Arrows show direction of (small) displacements of the apical domain in noncrystallographically related molecules.

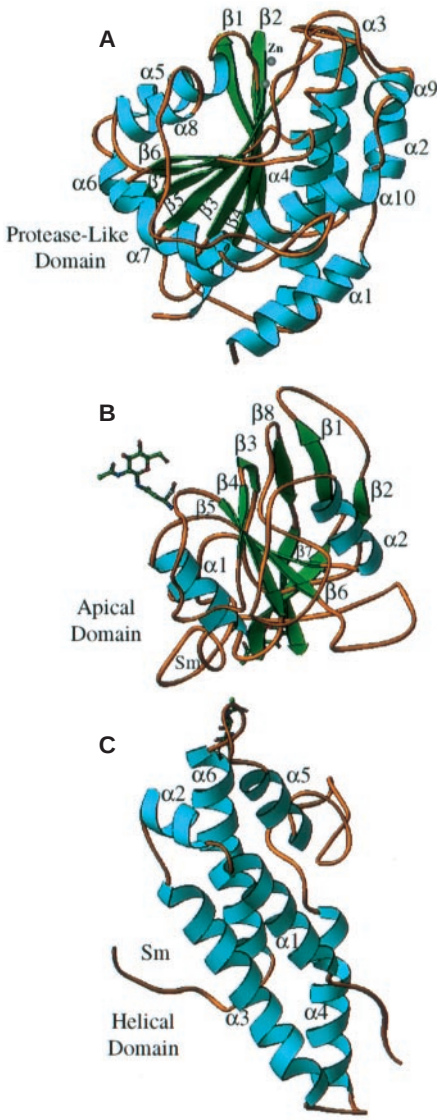

Fig. 2. Individual TfR domains. Ribbon diagrams for domain I, the protease-like domain (**A**); domain II, the apical domain (**B**); and domain III, the helical domain (**C**). Secondary structure elements are labeled. In the text, we refer to these elements first with respect to domain number and then with respect to the linear order of the element within the domain. For example, αI-3 refers to the third helix within the first domain. In (A), the two gray spheres indicate the positions that would be occupied by Zn^{2+} in an authentic protease.

A structure-based alignment of TfR (see Fig. 3 for amino acid sequence) and mGCP (*18*) reveals significant sequence identity (30.3%, 30.2%, and 24.0% for the protease-like, apical, and helical domains, respectively), but mGCP appears to lack much of the TfR stalk as well as the COOH-terminal tail that follows αIII-6. The catalytic site is covered by the apical domain, but the position of the αI-7/αI-8 loop allows access through an interdomain channel (Fig. 2A). The homologs of mGCP probably extend further in the evolutionary tree than does TfR itself, and it is possible that TfR arose from a cell-surface protease, perhaps one that recycled in and out of endosomes.

How might TfR bind Tf? We can model this interaction on the basis of the structural characteristics of the two proteins and the available functional information. A TfR dimer binds two Tf molecules, probably noncooperatively. Transferrin has two very similar lobes (N and C), each composed of two structurally dissimilar domains (N_1 and N_2; C_1 and C_2) (*19*). Each lobe chelates a single Fe^{3+} between the two domains. Iron release is accompanied by a substantial opening of the interdomain cleft, at least in the N lobe and probably in both (*19, 20*). Because iron release in the endosome occurs without dissociation of Tf from TfR, the complex must withstand a hinge-like opening of both lobes. Studies with proteolytically derived or recombinant N and C lobes of Tf show that both lobes of Tf interact with TfR but that the interactions between the C lobe and TfR are much stronger (*21*). Indeed, the binding constant for a proteolytically derived C lobe is 1/10th that of intact Tf (*21*). Thus, we expect that Tf C- lobe–TfR contacts should be more extensive than Tf N-lobe–TfR contacts, with much of the interface presumably coming from one of the two C domains.

The TfR dimer has a strikingly convoluted surface (Fig. 4). There are lateral facing clefts and a bowl-like depression at the top of the molecule. The central bowl is too small to accommodate two noninterfering Tf monomers, but the lateral clefts are more likely sites of interaction. Each cleft lies within a single monomer, with all three domains contributing to its surface. The cleft opens inward toward what would be the catalytic site of a structurally related protease. We find apparent surface complementarity between Tf and the lateral clefts of TfR, which has allowed us to dock the two molecules by inspection, followed by rigid body refinement (*22*) (Fig. 4). Our model has several noteworthy features: (i) Most contacts with

Tf involve the C_1 domain, with additional contributions from the N_1 domain, particularly near its COOH-terminus. The N_2 and C_2 domains of Tf have only minor interactions with TfR, and the putative motions within each lobe of Tf upon iron release are easily tolerated. (ii) The largest continuous patch of conserved surface residues in human and rabbit Tf is at the interface in the model between the apical domain of TfR and the N_1 and C_1 domains of Tf. (iii) Glycosylation sites on both human and rabbit Tf, which are not involved in Tf–TfR interactions (*23*), point away from TfR. We believe that our criteria are quite restrictive and that the model incorporates good approximations to the relative orientations of Tf and TfR and their contacting surfaces.

TfR is likely to have conformational switches associated with changes in pH. Iron release at low pH from TfR-bound Tf is faster and more complete than from unliganded Tf; the receptor enhances iron dissociation (*24*). One of the Sm^{3+} sites in the TfR crystal structure lies between the apical and protease-like domains (Fig. 1B). The Sm^{3+} is liganded by conserved acidic residues, which are nearly buried at the domain interface. When the ion dissociates, rearrangement of the binding loop, which also participates in dimer contacts, and rotation of the apical domain are required to separate the carboxylates. We therefore propose that motions of the apical domain transduce pH changes into changes in the Tf binding cleft. Shifts in the position of the apical domain could influence the relative affinities of TfR for apo- and holo-Tf and thus the affinity of Tf for Fe^{3+}. For example, hinged motions of the apical domain, as shown by the arrows in Fig. 1B, stimulate iron release by favoring the apo conformation of Tf. More generally, the structure suggests that pH-dependent switching involves large-scale domain displacements and not just local electrostatic changes. We also expect that ligands at the vestigial protease active site could influence apical domain motions and thus affect Tf binding and iron delivery.

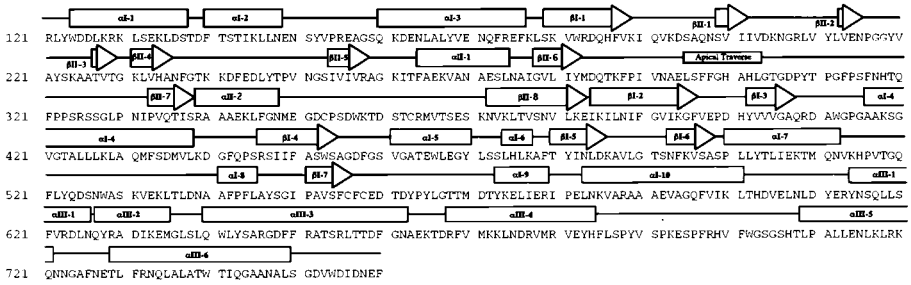

Fig. 3. Amino acid sequence of human TfR (*31*) with α helices and β strands indicated above the sequence by bars and arrows, respectively.

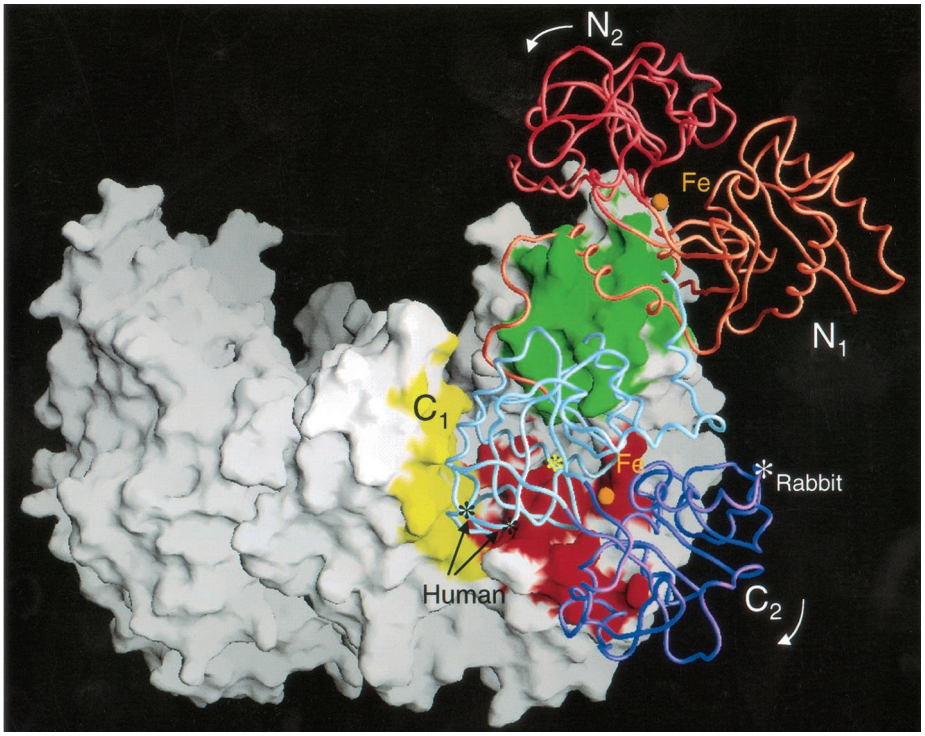

Fig. 4. Proposed model for binding of Tf to TfR receptor. The surface of the TfR dimer is rendered predominantly in white, with elements of the lateral cleft that are in contact with the docked Tf molecule colored according to domain as in Figs. 1 and 2 (the opening to the vestigial protease active site is indicated by a yellow asterisk). The structure of rabbit transferrin is shown as a worm, color coded by domain: first and second domains of the N lobe (N_1 and N_2) are orange and red, and the corresponding domains of the C lobe (C_1 and C_2) are blue and purple, respectively. Ferric ions are represented as labeled spheres, and the positions of human and rabbit N-linked glycosylation sites on Tf are denoted by white and black asterisks. White arrows indicate movements of the N_2 and C_2 domains upon ferric iron release. Docking of Tf to TfR, to model the complex, is described in the text. The model predicts that the following regions of TfR participate in binding Tf: the αII-2/βII-8 and βII-4/βII-5 loops of the apical domain, the αI-7/αI-8 loop of the protease-like domain, and αIII-1 and αIII-5 of the helical domain. Together, αIII-1 and αIII-5 form the COOH-terminal face of the lateral cleft, and these helices may contain residues responsible for species specificity of Tf association (*32*). The αI-7/αI-8 loop might also contribute to selectivity.

References and Notes

1. D. R. Richardson and P. Ponka, *Biochim. Biophys. Acta* **1331**, 1 (1997).
2. Abbreviations for amino acid residues are as follows: A, Ala; C, Cys; D, Asp; E, Glu; F, Phe; G, Gly; H, His; I, Ile; K, Lys; L, Leu; M, Met; N, Asn; P, Pro; Q, Gln; R, Arg; S, Ser; T, Thr; V, Val; W, Trp; Y, Tyr.
3. H. Fuchs, U. Lücken, R. Tauber, A. Engel, G. Reinhard, *Structure* **6**, 1235 (1998).
4. E. A. Rutledge, B. J. Root, J. J. Lucas, C. A. Enns, *Blood* **83**, 580 (1994).
5. S. Jing and I. S. Trowbridge, *EMBO J.* **6**, 327 (1987).
6. E. Alvarez, N. Girones, R. Davis, *ibid.* **8**, 2231 (1989).
7. A. P. Turkewitz, J. F. Amatruda, D. Borhani, S. C. Harrison, A. L. Schwartz, *J. Biol. Chem.* **263**, 8318 (1988); A. P. Turkewitz, A. L. Schwartz, S. C. Harrison, *ibid.*, p. 16309; D. W. Borhani and S. C. Harrison, *J. Mol. Biol.* **218**, 685 (1991).
8. J. N. Feder *et al., Proc. Natl. Acad. Sci. U.S.A.* **95**, 1472 (1998); S. Parkkila *et al., ibid.* **94**, 13198 (1997); J. A. Lebron *et al., Cell* **93**, 111 (1998).
9. C. N. Roy, D. M. Penny, J. N. Feder, C. A. Enns, *J. Biol. Chem.* **274**, 9022 (1999).
10. R. E. Carter, A. R. Feldman, J. T. Coyle, *Proc. Natl. Acad. Sci. U.S.A.* **93**, 749 (1996); R. E. Luthi-Carter, U. V. Berger, A. K. Barczak, M. Enna, J. T. Coyle, *ibid.* **95**, 3215 (1998).
11. T. Bzdega *et al., J. Neurochem.* **69**, 2270 (1997); N. D. Rawlings and A. J. Barrett, *Biochim. Biophys. Acta* **1339**, 247 (1997).
12. To express a recombinant form of the ectodomain of human TfR in CHO cells, we fused residues 117 to 760 of TfR to the COOH-terminal side of residues 1 to 34 of the preprolactin signal sequence. We placed this construct in a plasmid derived from pCMV4 (*25*), yielding pCMVTfR. Calcium phosphate cotransfection of CHO cells with pCMVTfR and pSV2neo allowed for selection and isolation of stably transformed cell lines secreting TfR. We grew CHO cells in Ham's- F-12 medium with 5% fetal bovine serum, penicillin, streptomycin, and G-418 (400 mg/ml). For large-scale expression, medium was harvested from roller bottles at 5-day intervals and centrifuged to pellet debris. The TfR was affinity purified from the supernatant as described (*7*) and stored at −80°C, yielding 2 mg of soluble TfR per liter of harvested medium. Before crystallization, TfR was treated with trypsin to remove eight NH_2-terminal residues (four vector-derived and TfR 117 to 120) as follows. The TfR

(4 mg) was concentrated by vacuum dialysis against 100 mM KCl, 100 mM NaCl, 5 mM potassium phosphate (pH 6.7) (buffer A) to a final concentration of 1 to 2 mg/ml. TfR was removed and placed on ice, and 20 ml of trypsin (10 mg/ml) was added. After 1 hour, TfR was passed over a benzamidine Sepharose column, and phenylmethysulfonyl fluoride was added (up to 1 mM) to inhibit residual trypsin activity. We then passed the TfR over a Superdex 200 size-exclusion column equilibrated with buffer A to remove aggregated protein.

13. For crystal growth, we concentrated TfR to about 12.5 mg/ml in buffer A. Hanging drops were assembled with 2 ml of TfR and 1 ml of well solution. Wells contained 2.3 to 2.5 M KCl, 10 mM KP_i, and either 1.5 to 2.0% polyethylene glycol (PEG) 6K or 1.2 to 2.0% PEG 20K. Crystals up to 0.5 × 0.4 × 0.3 mm grew over a 3- to 4-week period. Crystals were flash frozen by plunging into liquid N_2 or melting propane. The space group is $P2_12_12_1$, a = 105.4 Å, b = 216.9 Å, c = 361.9 Å. The asymmetric unit contains four TfR dimers, stacked along an 8_5 screw axis coincident with the crystallographic 2_1 parallel to c. Crystals soaked in 1 mM $SmCl_3$ for 24 hours diffracted significantly better than $SmCl_3$-free crystals; $SmCl_3$-soaked crystals were therefore used as native. A real-space heavy-atom search incorporating fourfold noncrystallographic symmetry (NCS) was used to find 16 heavy-atom positions in a di-μ-iodobis(ethylenediamine)diplatinum nitrate derivative (PIP) at 7.0 Å resolution. Single-isomorphous-replacement phases were then used in difference Fourier calculations to find 24 Sm^{3+} positions. Double-isomorphous-replacement phases were calculated by using PIP and $SmCl_3$-free data sets; for the latter, we refined negative Sm^{3+} occupancies. With iterative eightfold averaging and solvent flattening, the phases were refined at 6.0 Å resolution and extended to 3.2 Å. Data were collected on beamline F-1 at the Cornell High-Energy Synchrotron Source (CHESS) either on image plates or on the Quantum-4 CCD detector. All data were processed with the HKL suite (*26*). The data set (from Sm^{3+}-soaked crystals) used for refinement of the model has an overall R_{sym} of 9.9%. The data are essentially complete to 4.0 Å, falling to 32% complete in the outer shell from 3.25 to 3.2 Å, with an R_{sym} for the outer shell of 33.7%. Initial phases were calculated with MLPHARE (*27*), density modification was done with the program DM (*27*), and the model was built with O (*28*). The model has been refined with XPLOR (*22*) using tight NCS restraints (300 Kcal/mol Å^2) with the exception of crystallographic contacts. The apical domain was treated as an NCS group separate from the protease-like and helical domains. The current R_{cryst} and R_{free} for the refined model, using data from 8.0 to 3.2 Å with $I/\sigma(I) >$ 2.0, are 24.0% and 28.7%, respectively. The root-mean-square deviations in bond lengths and bond angles are 0.007 Å and 1.18°. Figs. 1 and 2 were drawn with RIBBONS (*29*), and Fig. 4 was drawn with GRASP (*30*).
14. Letters A to H designate the eight TfR monomers in the crystallographic asymmetric unit. The physiological dimers were identified by the proximity of their NH_2-termini. They are the four pairs AB, CD, EF, and GH related to each other by the 8_5 noncrystallographic symmetry. Each dimer interface has a large solvent-inaccessible surface area of 4100 Å^2. There are also significant contacts between successive dimers within the 8_5 helical columns (2600 Å^2).
15. A. M. Williams and C. A. Enns, *J. Biol. Chem.* **268**, 12780 (1993).
16. B. Chevrier, H. D'Orchymont, C. Schalk, C. Tarnus, D. Moras, *Eur. J. Biochem.* **237**, 393 (1996).
17. A. H. Robbins and C. D. Stout, *Proteins* **5**, 289 (1989).
18. Supplementary material is available at www.sciencemag.org/feature/data/1043272.shl
19. S. Bailey *et al., Biochemistry* **27**, 5804 (1988).
20. B. F. Anderson, H. M. Baker, G. E. Norris, S. V. Rumball, E. N. Baker, *Nature* **344**, 784 (1990); B. J. Anderson, H. M. Baker, G. E. Norris, D. W. Rice, E. N. Baker, *J. Mol. Biol.* **209**, 711 (1989); P. D. Jeffrey *et al., Biochemistry* **37**, 13978 (1998).
21. O. Zak, D. Trinder, P. Aisen, *J. Biol. Chem.* **269**, 7110 (1994); A. B. Mason *et al., Biochem. J.* **326**, 77 (1997).
22. A. T. Brunger, *X-PLOR Version 3.0: A System for Crystallography and NMR* (Yale University Press, New Haven, CT, 1992).
23. S. Kornfield, *Biochemistry* **7**, 945 (1968); D. Hemmaplardh and E. H. Morgan, *Biochim. Biophys. Acta* **426**, 385 (1976); A. B. Mason *et al., Biochemistry* **32**, 5472 (1993).
24. P. K. Bali, O. Zak, P. Aisen, *Biochemistry* **30**, 324 (1991); D. Sipe and R. Murphy, *J. Biol. Chem.* **266**, 8002 (1991).
25. S. Andersson, D. Davis, H. Dahlbäck, H. Jörnvall, D. Russell, *J. Biol. Chem.* **264**, 8222 (1989).
26. Z. Otwinowski and W. Minor, *Methods Enzymol.* **276**, 307 (1997).
27. CCP4, *Acta Crystallogr. D* **50**, 760 (1994).
28. T. A. Jones, J.-Y. Zou, S. W. Cowan, M. W. Kjelgard, *Acta Crystallogr. A* **47**, 110 (1991).
29. M. Carson and C. E. Bugg, *J. Mol. Graph.* **4**, 121 (1986).
30. A. Nichols, K. A. Sharp, B. Honig, *Proteins Struct. Funct. Genet.* **11**, 282 (1991).
31. C. Schneider, M. J. Owen, D. Banville, J. G. Williams, *Nature* **311**, 675 (1984); A. McClelland, L. C. Kuhn, F. H. Ruddle, *Cell* **39**, 267 (1984).
32. F. Buchegger, I. S. Trowbridge, L. S. Liu, S. White, J. F. Collawn, *Eur. J. Biochem.* **235**, 9 (1996).
33. We thank D. Thiel and other staff members at CHESS for assistance with data collection at the F-1 beamline; W. Minor for help in data processing; R. Davis for help with CHO cell expression; P. Aisen, N. Andrews, M. Eck, and M. Wessling-Resnick for discussion; and P. Bjorkman, M. Bennet, and C. Enns for communicating results before publication. C.M.L. is an Armenise Fellow of the Harvard Medical School Center for Structural Biology.

7 July 1999; accepted 8 September 1999

Microtubule Disassembly by ATP-Dependent Oligomerization of the AAA Enzyme Katanin

James J. Hartman and Ronald D. Vale*

Katanin, a member of the AAA adenosine triphosphatase (ATPase) superfamily, uses nucleotide hydrolysis energy to sever and disassemble microtubules. Many AAA enzymes disassemble stable protein-protein complexes, but their mechanisms are not well understood. A fluorescence resonance energy transfer assay demonstrated that the p60 subunit of katanin oligomerized in an adenosine triphosphate (ATP)– and microtubule-dependent manner. Oligomerization increased the affinity of katanin for microtubules and stimulated its ATPase activity. After hydrolysis of ATP, microtubule-bound katanin oligomers disassembled microtubules and then dissociated into free katanin monomers. Coupling a nucleotide-dependent oligomerization cycle to the disassembly of a target protein complex may be a general feature of ATP-hydrolyzing AAA domains.

Microtubules, polymers of α- and β-tubulin subunits, form the mitotic spindle and organize membranous organelles in interphase cells. To accomplish these disparate functions, the microtubule cytoskeleton must rapidly reorganize into different configurations. Microtubules undergo spontaneous growth and shrinkage at their ends, even at steady state, which is important for the cellular rearrangements of these polymers (*1, 2*). In addition to end dynamics, the microtubule wall can be disrupted by the severing enzyme katanin (*3*). Potential in vivo roles for katanin-mediated microtubule severing include releasing microtubules from centrosomes (*4*), depolymerizing microtubule minus ends in the mitotic spindle as a component of poleward flux (*5*), and accelerating microtubule turnover at the G_2/M transition of the cell cycle by creating unstable microtubule ends (*6*).

Katanin is a microtubule-stimulated ATPase, and ATP hydrolysis is required for it to sever and disassemble stable microtubules (*3*). Katanin is a heterodimer organized into a 60-kD enzymatic subunit (p60), which carries out the ATPase and severing reactions, and a targeting subunit (p80), which localizes katanin to the centrosome (*7*). The sequence of p60 reveals that it belongs to the AAA ATPase superfamily, members of which share one or two copies of a conserved 230-amino acid ATPase domain (*8–10*). AAA proteins have been implicated in a myriad of cellular processes as diverse as membrane targeting (NSF, VPS4, p97), organelle biogenesis (PAS1p), proteolysis (SUG1), and transcriptional regulation (TBP1) (*11*). AAA proteins have been proposed to act as nucleotide-dependent chaperones that can disassemble specific protein complexes or unfold polypeptides (*8*). However, little is known about how changes in the nucleotide state of the AAA domain are coupled to the disassembly of their protein targets.

Like the AAA protein NSF (*12, 13*), p60 katanin can form 14- to 16-nm rings, as shown by electron microscopy (*7*). However, p60 (*14*) and GFP-p60, a chimeric protein composed of green fluorescence protein and p60, migrated primarily as 4*S* monomers in 10% to 35% glycerol gradients in the presence of ATP, adenosine diphosphate (ADP), or adenosine-5′-(γ-thio)triphosphate (ATP-γ-S) (Fig. 1A) (*15*).

The Howard Hughes Medical Institute and the Department of Cellular and Molecular Pharmacology, University of California, San Francisco, CA 94143, USA.

*To whom correspondence should be addressed. E-mail: vale@phy.ucsf.edu